

# **Coupling of a Bladed Hub to the Tower of the Ampair 600 Wind Turbine using the Transmission Simulator Method**

Daniel P. Rohe and Randy L. Mayes  
Experimental Mechanics, NDE and Model Validation Department  
Sandia National Laboratories\*  
P.O. Box 5800 - MS0557  
Albuquerque, NM, 87185  
dprohe@sandia.gov  
rlmayes@sandia.gov

## **ABSTRACT**

This paper presents an example of the transmission simulator method of experimental dynamic substructuring combining two substructures of the Substructures Focus Group's test bed, the Ampair 600 Wind Turbine. The two substructures of interest are the hub-and-blade assembly and the tower assembly that remains after the hub is removed. The hub-and-blade substructure was developed from elastic modes of a free-free test of the hub and blades, and rigid body modes were constructed from measured mass properties. Elastic and rigid body modes were extracted from experimental data for the tower substructure. A bladeless hub was attached to the tower to serve as the transmission simulator for this substructure. Modes up to the second bending mode of the blades and tower were extracted. Substructuring calculations were then performed using the transmission simulator method, and a model of the full test bed was derived. The combined model was compared to truth data from a test on the full turbine.

## **KEYWORDS**

Experiment; MCFS; Substructuring; Transmission Simulator; Wind Turbine;

## **1. Introduction**

Dynamic substructuring gives an analyst the ability to predict the response of a built up system based on the responses of its subcomponents. This is particularly useful when the final system is too large or complex to test as one piece, or when design constraints require the redesign of one component while others remain the same, especially if the designing group has little control over the component to which their component attaches. This effort focuses on a wind turbine structure where a subsystem containing the blades is coupled to a subsystem containing the tower and nacelle. One can imagine a scenario in which a turbine tower is erected, but the boundary conditions of the tower are not well known due to uncertainties in soil properties or other factors. It may be easier to experimentally test the tower than to accurately model the interaction between the base of the tower and the ground, then couple the experimental model of the tower to a model containing the blades of the system. This way any problematic modes may be discovered before the system is assembled, allowing the potential for structural modification of either system.

The transmission simulator method of experimental dynamic substructuring is used in this effort. This method offers distinct advantages over other substructuring methods, but it can be more expensive to perform because it requires an additional component—the transmission simulator. However, in this case this expense is avoided by using a component of the turbine system as the transmission simulator, which reduces the cost of the test as the component should be readily available. This allows the transmission simulator method to be comparable in effort to other methods of substructuring.

## **2. Test Objectives and Methods**

The objective of these tests is to create a substructured model of the Ampair 600 Wind Turbine assembled from component models of the tower and a blades-and-hub structure. This model will be compared to an experimental 'truth' model from a

\*Sandia is a multiprogram laboratory operated by Sandia Corporation, a Lockheed Martin Company, for the U.S. Department of Energy under Contract DE-AC04-94AL85000.

modal test of the entire assembled structure. Of interest in these experiments were the modes up to the second bending modes of the tower and blades. Previous tests containing these structures in similar configurations [1, 2] showed that the highest frequencies of interest would occur near 100 Hz. The test range was set from 0 to 156.25 Hz to allow these modes (and a few higher) to be captured.

For each test, a 0.3 kg (0.7 lb) impact hammer with the softest available tip was used to excite the structures' elastic modes. The modes were extracted with the SMAC algorithm [3].

The pitch, roll, and yaw rotations as used in this paper are defined as the rotations about the  $x$ ,  $z$ , and  $y$  directions, respectively, as shown in Figure 1. The origin of the coordinate system is defined as the tip of the hub, placing the majority of the structure in the  $-z$  direction.

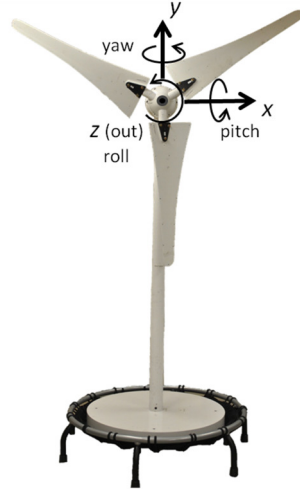


**Figure 1: Global coordinate system and rotation definitions.**

### 3. Test Structures

Tests were performed on two different substructures in order to assemble them into the complete Ampair turbine structure. The first structure was the hub, disconnected from the nacelle at the mock generator shaft, with the blades attached. The second substructure was the turbine with the hub locked to the parked shaft and the blades removed. Both structures are shown in Figure 2. Since both structures include the hub, one will need to be subtracted as is common in the transmission simulator method.



**Figure 2: Structures tested to perform substructuring. (a) Bladeless tower (left) and (b) hub and blades (right)**

### 3.1. Bladeless Tower Test

#### 3.1.1. Test Setup

Mode shapes from previous tests revealed rough location for tower nodes, which would need to be avoided when placing accelerometers. The tower was instrumented such that the first and second bending shapes of the tower would be visible and distinguishable from one another. The hub and nacelle were both instrumented such that relative rigid body motions between the two components would be visible, and the tail was instrumented to distinguish flapping and torsion modes. The massive base of the tower was instrumented with four high-sensitivity (500 mV/g) accelerometers because its motion tended to be very small due to its large mass. Accelerometer locations and a line model are shown in Figure 3.

The structure was excited at a large number of drive points in order to ensure that all of the modes were excited adequately. The tower was impacted to excite pole bending modes. Several drive points were chosen on the transmission simulator, both on the arms (white) and on the clamps (black). The lower tail point was also excited.

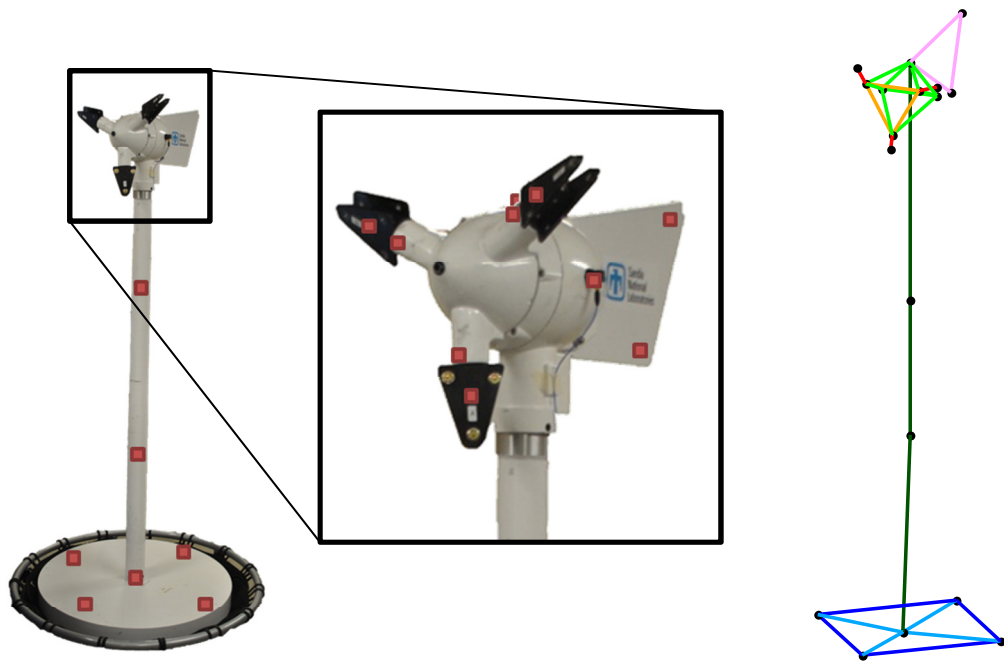


**Figure 3: Instrumentation locations for the Tower structure.**

The tower structure rests upon a commercial trampoline. Previous work [1] has shown that the lowest elastic modes near 20 Hz are only about 5 times higher in frequency than the highest rigid body modes near 4 Hz, whereas the desired ratio is typically 10 times or more. Therefore, considering this system to be a 'free-free' approximation may not be an adequate assumption. Also, precise mass properties for this structure, from which properly-scaled rigid body modes could be reconstructed, were not known. However, in many studies it has been seen that properly-scaled rigid body modes play an integral part in substructuring calculations [4,5]. For these reasons, the rigid body modes of the structure were measured experimentally in a separate test.

The rigid body modes were excited via a swept-sine shaker input to the base and tower of the structure (Figure 4). From these inputs, all six rigid body modes could be excited. Since the frequencies were on the order of just a few Hz, the test was operating on the lower end of the accelerometers' sensitivity. This led to mode shapes which were slightly noisy. To average out these small errors, rigid body modes were constructed from the three principal rotations and three principal translations and then fit to the experimental data in a least-squares fashion. This effort gave smooth, scaled rigid body shapes that matched the frequencies from [1] well. These modes were appended to the elastic modes from the impact test to derive a full modal model of the tower.



**Figure 4: Drive points to excite rigid body modes: Tower for pitching and rolling modes (left) and base for yawing (top right) and y-direction bounce (bottom right).**

### 3.1.2. Results

Six rigid body modes and seven elastic modes were extracted from the data in the test range. The natural frequencies and damping ratios for each mode are shown in Table 1.

Mode	Frequency (Hz)	Damping Ratio (%)	Description
1	0.89	1.62	z-direction Translation
2	0.95	3.64	x-direction Translation
3	2.83	8.24	y-direction Translation
4	3.04	2.90	Yaw Mode
5	3.25	6.57	Pitch Mode
6	3.93	6.69	Roll Mode
7	20.53	1.01	1 <sup>st</sup> Bending in yz-plane
8	20.55	0.95	1 <sup>st</sup> Bending in xy-plane
9	46.84	0.25	Pole Torsion Mode
10	73.89	0.70	2 <sup>nd</sup> Bending in yz-plane
11	84.59	0.70	2 <sup>nd</sup> Bending in xy-plane
12	96.75	0.30	Tail Flapping Mode
13	148.87	1.50	Generator Shaft Torsion

**Table 1: List of extracted modes from the tower test.**

The analytical model was a good fit to the experimental data. This can be attributed to the simplicity of the turbine tower system, which resembles a beam with large masses on both ends. Good data was generally taken from impacting the pole and transmission simulator. Data from tail impacts tended to not look as good. Since the tail is quite soft compared to the rest of the system, an adequate force level on the tail would result in large deformations, which resulted in slightly nonlinear

behavior. Additionally, this large displacement made it difficult to impact the structure without double hits. Complex mode identifier functions (CMIFs) from pole and tail impacts are shown in Figure 5.

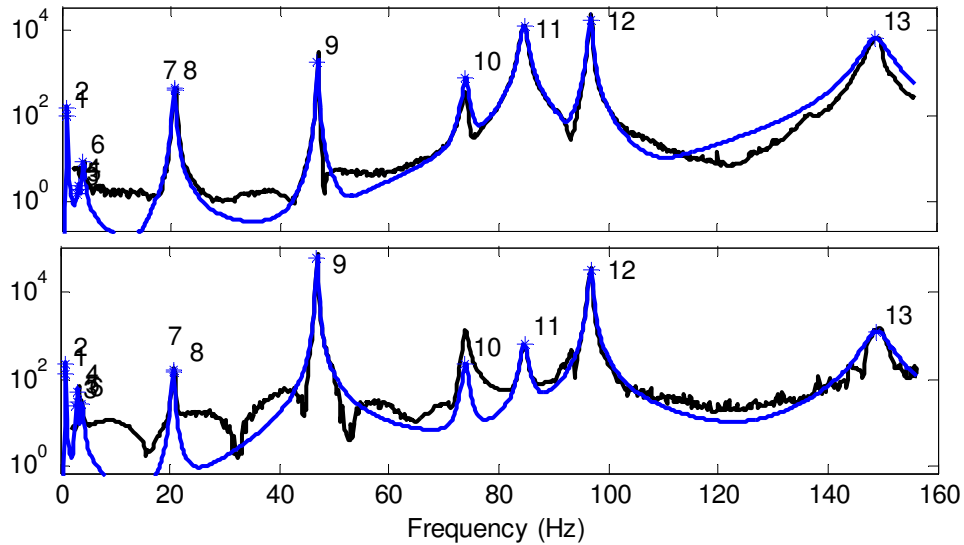


**Figure 5: CMIFs from a pole reference (top) and the tail reference (bottom). Experimental data is shown in black, and the analytical fit is shown in blue.**

### 3.2. Hub and Blades Test

#### 3.2.1. Test Setup

For the hub and blade structure, the transmission simulator was instrumented identically as for the tower structure test. Each blade was instrumented with two triaxial accelerometers to identify first and second bending and edgewise modes. Torsion modes would not be easily identifiable in this configuration; however, recent tests on the blades [2] suggest that these modes will be out of the frequency range of interest. The accelerometer locations and a line model are shown in Figure 6.

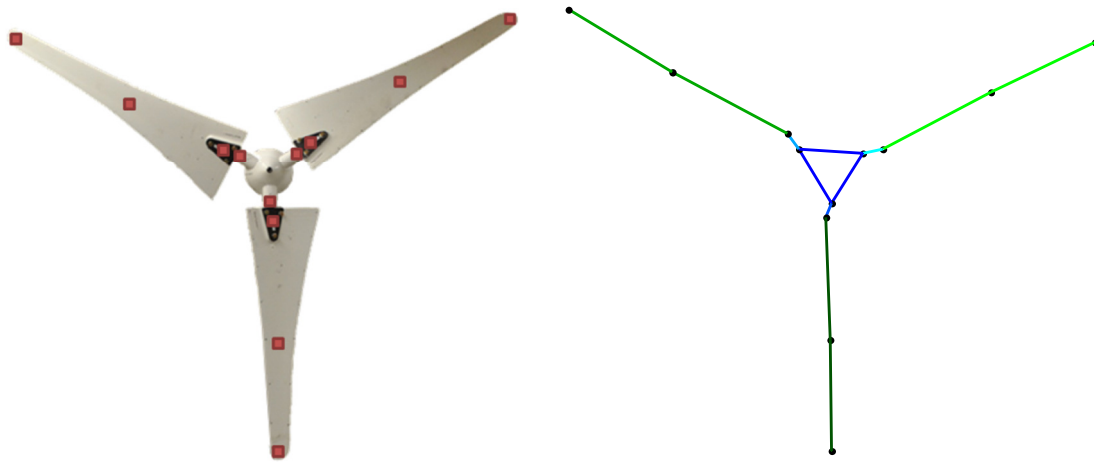


**Figure 6: Instrumentation locations for the Hub and Blades**

The structure was excited at drive points on the transmission simulator and near the midpoint of the blade. The blade tips did not work well as a drive point as the large deflection of the blade tip made it difficult not to double-hit the structure.

Because the hub was supported on soft springs, the rigid body modes were too low in frequency to measure via modal test with the current setup. The rigid body modes of the system needed to be constructed from mass properties. Mass properties from the hub were measured experimentally on a Space Electronics mass properties machine, and mass properties for the three blades were estimated from the CAD geometry presented in [6]. Three blades were arranged as they would be in the

assembly, and mass properties were calculated by the Solidworks modeling software shown in Figure 7. It was assumed that the blade's base (highlighted in blue in Figure 7) and the blade's span (shown in gray in Figure 7) had unique but uniform densities, and each density was tuned so that the total mass and center of gravity along the span were consistent with a simple balancing experiment. The calculated densities of each portion of the blade are given in Table 2.

Blade Span	940.5 kg/m <sup>3</sup>
Blade Base	2664.5 kg/m <sup>3</sup>

**Table 2: Blade approximate densities**

The mass properties of the blades and the hub were combined using the parallel axis theorem. Rigid body modes shapes were created from the three principal translations and rotations, and scaled using the calculated mass properties.

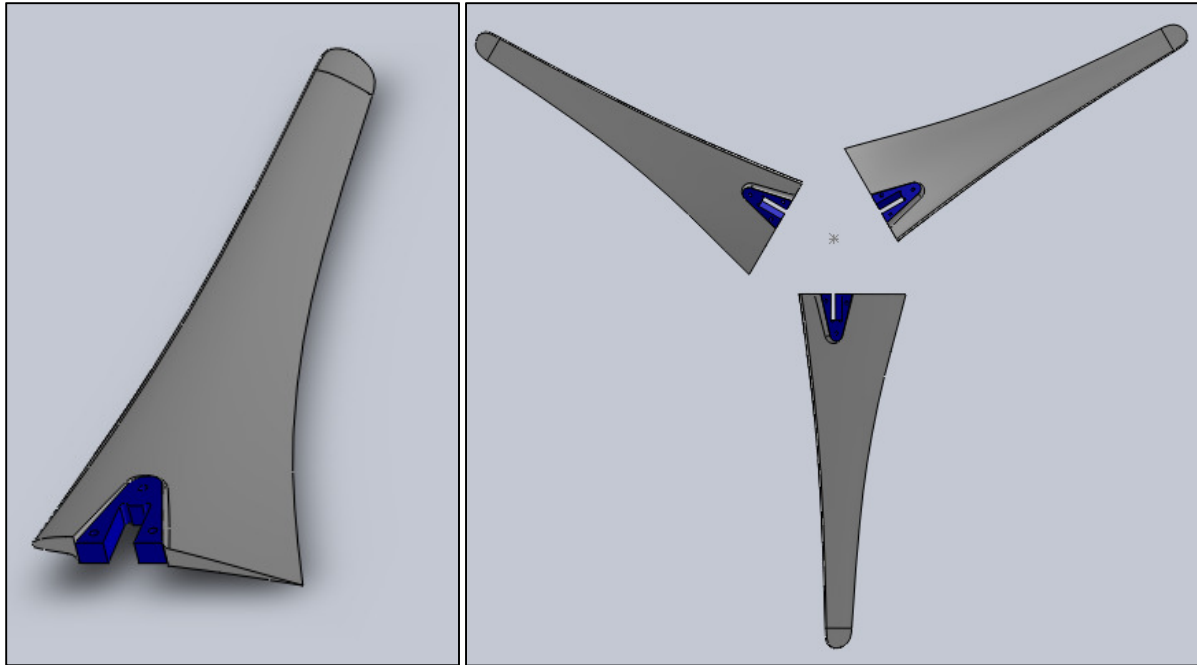


**Figure 7: Blade solid models based on measured blade geometry.**

Property	Hub	Three Blades	Entire Rotor
Mass	3.6 kg	2.6 kg	6.2 kg
$c_{g,z}$	-0.0615 m	-0.0673 m	-0.0637 m
$I_{xx}$	0.0150 kg-m <sup>2</sup>	0.189 kg-m <sup>2</sup>	0.204 kg-m <sup>2</sup>
$I_{yy}$	0.0148 kg-m <sup>2</sup>	0.189 kg-m <sup>2</sup>	0.204 kg-m <sup>2</sup>
$I_{zz}$	0.0276 kg-m <sup>2</sup>	0.3769 kg-m <sup>2</sup>	0.405 kg-m <sup>2</sup>

**Table 3: Mass Properties.** Moments of inertia are measured from the center of mass of each object. Since all have rotational symmetry about z, all cross products of inertia are zero, and all  $c_g$  lie on the z-axis.

### 3.2.2. Results

The six analytically generated rigid body modes were combined with nine elastic modes extracted from the impact tests. These modes are enumerated in Table 4.

Mode	Frequency (Hz)	Damping Ratio (%)	Description
1	0.1 *	0	$x$ -direction Translation
2	0.1 *	0	$y$ -direction Translation
3	0.1 *	0	$z$ -direction Translation
4	0.1 *	0	Rigid Body Yaw
5	0.1 *	0	Rigid Body Pitch
6	0.1 *	0	Rigid Body Roll
7	20.36	2.17	1 <sup>st</sup> Bending, 3 Blades in Phase
8	27.27	1.75	1 <sup>st</sup> Bending, 1 Blade out of Phase
9	28.97	1.84	1 <sup>st</sup> Bending, 1 Blade out of Phase
10	53.19	3.27	2 Blade Edgewise Mode
11	62.14	1.81	2 Blade Edgewise Mode
12	68.38	1.76	2 <sup>nd</sup> Bending, 3 Blades in Phase
13	95.31	2.14	2 <sup>nd</sup> Bending, 1 Blade out of Phase
14	100.05	1.50	2 <sup>nd</sup> Bending, 1 Blade out of Phase
15	153.09	2.49	3 Blade Edgewise Mode

**Table 4: List of extracted modes from Blade and Hub test. (\*) Note that the rigid body modes were given small positive frequencies to ensure that no negative mass or stiffness developed from the subtraction.**

Due to the nature of the connections of this substructure, it behaved less linearly than the tower structure tested previously. The blades are attached to the hub via features that clamp the blade when tightened. These joints, relying primarily on friction, will slip if a large enough excitation is applied. Similar to the tower, when the structure was excited on the stiffer transmission simulator, the smaller response gave more linear results. Exciting at the blades' midspan gave strong bending responses, but apparently more nonlinear response. The focus here was to fit the strongest resonances below 100 Hz (see Figure 8).

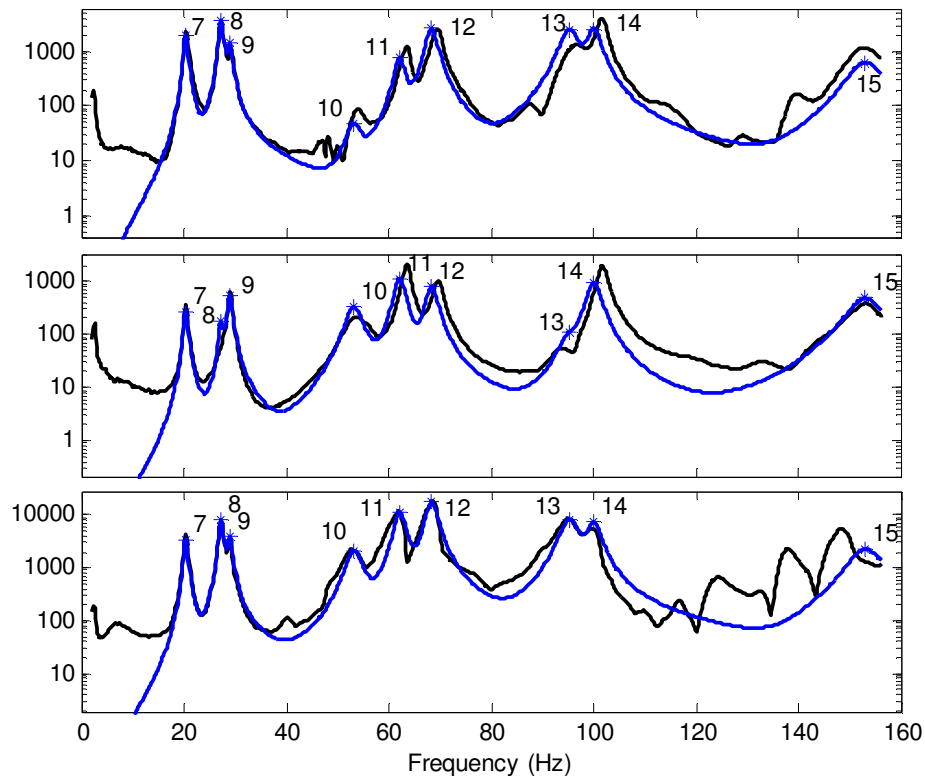


**Figure 8: CMIFs of the Blade and Hub structure. References from top to bottom:  $z$ -direction on Transmission Simulator;  $y$ -direction on Transmission Simulator, edgewise modes are excited better;  $z$ -direction on blade, strong bending excitation, but nonlinear effects in high frequency range. Experimental data is black and the analytical fit is blue.**

#### 4. Substructuring Methodology

The transmission simulator method was used to assemble the systems presented above with the turbine hub as the transmission simulator. The transmission simulator method offers distinct advantages over the conventional method of constraining individual degrees of freedom at the interface. Specifically, if one did not have a transmission simulator loading up the free end of the shaft, there would be no tip loads or moments developed on that free end due to the free boundary condition. This, combined with its lack of length, would cause the shaft to behave rigidly in every mode in the band of interest. No joint flexibility or damping would be captured. Additionally, the analyst may have trouble capturing the rotations of the end of the shaft accurately. The transmission simulator method mass-loads the shaft and implicitly captures the rotations of the connection point providing a much better set of basis vectors than free modes without the hub.

For this experiment, the transmission simulator contained 15 degrees of freedom, 5 on each blade anchor. Through a quick tap test, it was found that the first elastic mode of the transmission simulator had a natural frequency near 1200 Hz, which was far above the frequency range of the test. Therefore, the transmission simulator was assumed to be rigid over the frequency band of interest. The transmission simulator model used in substructuring calculations contained only 6 rigid body modes—the three principal translations and rotations—created from the measured mass properties of the hub shown in Table 3.

The substructuring calculations then proceed. For the following, the subscript  $t$  represents the tower-and-hub structure; the subscript  $b$  represents the blades-and-hub structure; and the subscript  $TS$  represents the transmission simulator structure (hub).  $\Phi$  represents the mode shapes of each system,  $\omega$  represents the natural frequencies, and  $\zeta$  represents the damping ratios. The  $\mathbf{x}_i$  vectors represent physical degrees of freedom on subsystem  $i$ , where  $\mathbf{q}_i$  represent modal degrees of freedom. A subscript  $m$  denotes the subset of measured physical degrees of freedom that exist on the transmission simulator in each substructure.

Starting with all three systems (tower, blades, and a *negative* transmission simulator) concatenated in the typical mass-normalized modal representation of the equations of motion

$$\begin{bmatrix} \mathbf{I}_t & 0 \\ 0 & \mathbf{I}_b & -\mathbf{I}_{TS} \end{bmatrix} \begin{Bmatrix} \ddot{\mathbf{q}}_t \\ \ddot{\mathbf{q}}_b \\ \ddot{\mathbf{q}}_{TS} \end{Bmatrix} + \begin{bmatrix} [2\zeta_t\omega_t] & 0 \\ 0 & [2\zeta_b\omega_b] & -[2\zeta_{TS}\omega_{TS}] \end{bmatrix} \begin{Bmatrix} \dot{\mathbf{q}}_t \\ \dot{\mathbf{q}}_b \\ \dot{\mathbf{q}}_{TS} \end{Bmatrix} + \begin{bmatrix} [\omega_t^2] & 0 \\ 0 & [\omega_b^2] & -[\omega_{TS}^2] \end{bmatrix} \begin{Bmatrix} \mathbf{q}_t \\ \mathbf{q}_b \\ \mathbf{q}_{TS} \end{Bmatrix} = \begin{Bmatrix} \Phi_t^T \mathbf{F}_t \\ \Phi_b^T \mathbf{F}_b \\ \Phi_{TS}^T \mathbf{F}_{TS} \end{Bmatrix} \quad (1)$$

the constraints on the system can be assembled. These constraints equate the motion of the transmission simulator in each substructure.

$$\begin{bmatrix} \mathbf{I} & 0 & -\mathbf{I} \\ 0 & \mathbf{I} & -\mathbf{I} \end{bmatrix} \begin{Bmatrix} \mathbf{x}_{t,m} \\ \mathbf{x}_{b,m} \\ \mathbf{x}_{TS,m} \end{Bmatrix} = \mathbf{0} \quad (2)$$

Casting equation (2) into modal coordinates gives

$$\begin{bmatrix} \mathbf{I} & 0 & -\mathbf{I} \\ 0 & \mathbf{I} & -\mathbf{I} \end{bmatrix} \begin{bmatrix} \Phi_{t,m} & 0 \\ 0 & \Phi_{b,m} & \Phi_{TS,m} \end{bmatrix} \begin{Bmatrix} \mathbf{q}_t \\ \mathbf{q}_b \\ \mathbf{q}_{TS} \end{Bmatrix} = \mathbf{0} \quad (3)$$

or

$$\begin{bmatrix} \Phi_{t,m} & 0 & -\Phi_{TS,m} \\ 0 & \Phi_{b,m} & -\Phi_{TS,m} \end{bmatrix} \begin{Bmatrix} \mathbf{q}_t \\ \mathbf{q}_b \\ \mathbf{q}_{TS} \end{Bmatrix} = \mathbf{0} \quad (4)$$

The transmission simulator method transforms the physical constraints to softer modal constraints by pre-multiplying the equation by the pseudo-inverse of the transmission simulator mode shapes



$$\begin{bmatrix} \Phi_{TS,m}^+ & 0 \\ 0 & \Phi_{TS,m}^+ \end{bmatrix} \begin{bmatrix} \Phi_{t,m} & 0 \\ 0 & \Phi_{b,m} \end{bmatrix} \begin{bmatrix} -\Phi_{TS,m} \\ -\Phi_{TS,m} \end{bmatrix} \begin{Bmatrix} \mathbf{q}_t \\ \mathbf{q}_b \\ \mathbf{q}_{TS} \end{Bmatrix} = \mathbf{0} \quad (5)$$

The two left-most matrices can be collected to form a single matrix that specifies the constraints on the modal degrees of freedom  $\mathbf{q}_i$ .

$$\mathbf{A} \begin{Bmatrix} \mathbf{q}_t \\ \mathbf{q}_b \\ \mathbf{q}_{TS} \end{Bmatrix} = \mathbf{0} \quad (6)$$

The uncoupled set of modal degrees of freedom  $\mathbf{q} = \{\mathbf{q}_t \quad \mathbf{q}_b \quad \mathbf{q}_{TS}\}^T$  can be transformed into a coupled set through some transformation  $\{\mathbf{q}\} = [\mathbf{L}]\{\mathbf{q}_u\}$ . By substituting this transformation into (6) it becomes clear that  $\mathbf{L}$  must reside in the null space of  $\mathbf{A}$  since  $\mathbf{q}_u$  is generally not zero. That is,  $\mathbf{L}$  must be orthogonal to  $\mathbf{A}$  so that

$$\mathbf{A}\mathbf{L}\mathbf{q}_u = \mathbf{0} \quad (7)$$

Substituting  $\mathbf{L}\mathbf{q}_u$  for  $\mathbf{q}$  in (1) and pre-multiplying by  $\mathbf{L}^T$  gives the coupled equations of motion for the system, from which eigenvalues, eigenvectors, and damping properties can be found.

$$\begin{aligned} \hat{\mathbf{M}}\ddot{\mathbf{q}}_u + \hat{\mathbf{C}}\dot{\mathbf{q}}_u + \hat{\mathbf{K}}\mathbf{q}_u &= \mathbf{Q} \\ \hat{\mathbf{M}} &= \mathbf{L}^T \begin{bmatrix} \mathbf{I}_t & & 0 \\ & \mathbf{I}_b & \\ 0 & & -\mathbf{I}_{TS} \end{bmatrix} \mathbf{L} \\ \hat{\mathbf{C}} &= \mathbf{L}^T \begin{bmatrix} [2\zeta_t \omega_{t,n}] & & 0 \\ & [2\zeta_b \omega_{b,n}] & \\ 0 & & -[2\zeta_{TS} \omega_{TS,n}] \end{bmatrix} \mathbf{L} \\ \hat{\mathbf{K}} &= \mathbf{L}^T \begin{bmatrix} [\omega_{t,n}^2] & & 0 \\ & [\omega_{b,n}^2] & \\ 0 & & -[\omega_{TS,n}^2] \end{bmatrix} \mathbf{L} \\ \mathbf{x} &= \begin{bmatrix} \Phi_t & & 0 \\ & \Phi_b & \\ 0 & & \Phi_{TS} \end{bmatrix} \mathbf{L}\mathbf{q}_u \end{aligned} \quad (8)$$

## 5. Substructuring Results

Coupling the systems together as described in the previous section, a full turbine model is derived. This substructured model is now compared to the results from the truth test on the entire turbine. This truth test used accelerometers in exactly the same locations as on the substructures, allowing a point-by-point comparison of the substructured turbine and the measured turbine.

Since the modes of the turbine were found to be closely spaced in previous work [1], an ad hoc sorting algorithm was implemented that would assign equivalent modes between the truth and substructured models. This would allow a correct comparison of the modes of the systems in case errors caused the modes to appear out-of-order or spurious computational modes developed like in [4]. This sorting algorithm assigns a numerical weight based on the value of the Modal Assurance Criterion (MAC) and the frequency error between the truth mode and substructured mode. While a straight MAC comparison would perform adequately to find similar modes, experience in [4] has shown that sometimes high frequency substructured mode shapes can look the same as correct low frequency modes and in rare circumstances can have a better MAC. By weighting by frequency error as well, this miscorrelation can often times be avoided. This was useful for mode 8 of the truth system in Figure 9. Based purely on MAC, substructured mode 13 would have been chosen, even though there is a substructured mode with a similar (though slightly worse) MAC near that frequency. The weight  $W_{ij}$  between the  $i$ th truth mode and the  $j$ th substructured mode is

$$W_{ij} = \text{MAC}(\Phi_{Truth,i}, \Phi_{Substr,j}) \cdot (1 - F \cdot |f_{Truth,i} - f_{Substr,j}|) \quad (9)$$

where  $F$  is a weight applied to the frequency error, in this case,  $F = 0.025$ . The highest weight  $W_{ij}$  for the  $i$ th truth mode is then said to correspond to that mode. The truth modes and their substructured complements are shown in Table 5. The MAC between the two systems is shown in Figure 9.

Truth Mode	Frequency (Hz)	Substr Match	Frequency (Hz)	Error	Truth Damping	Substr Damping	Error	MAC
Mode 1	17.24	Mode 1	17.86	3.58%	1.12%	0.99%	-12.08%	0.92
Mode 2	17.70	Mode 2	18.06	2.05%	0.78%	1.12%	44.53%	0.98
Mode 3	18.71	Mode 3	19.10	2.10%	0.81%	1.24%	52.68%	0.93
Mode 4	20.06	Mode 4	19.85	-1.02%	0.87%	1.32%	51.83%	0.97
Mode 5	21.46	Mode 5	21.21	-1.16%	0.92%	1.22%	32.93%	0.93
Mode 6	30.06	Mode 6	29.66	-1.32%	1.79%	0.44%	-75.37%	0.98
Mode 7	37.31	Mode 7	38.15	2.24%	1.00%	0.77%	-22.71%	0.99
Mode 8	48.38	Mode 8	51.27	5.98%	1.70%	2.65%	56.15%	0.62
Mode 9	54.87	Mode 9	56.92	3.74%	3.15%	1.40%	-55.52%	0.70
Mode 10	60.68	Mode 10	61.50	1.34%	1.96%	1.76%	-10.16%	0.83
Mode 11	66.16	Mode 11	66.31	0.21%	1.47%	1.70%	15.72%	0.72
Mode 12	68.60	Mode 12	75.41	9.93%	0.82%	0.77%	-6.58%	0.59
Mode 13	84.44	Mode 13	88.10	4.33%	0.92%	1.54%	66.43%	0.85
Mode 14	95.26	Mode 14	95.50	0.24%	1.14%	1.24%	9.15%	0.88
Mode 15	106.85	Mode 15	104.62	-2.09%	0.86%	0.92%	6.16%	0.93
Mode 16	121.28	-	-	-	1.15%	-	-	-
Mode 17	140.80	-	-	-	1.19%	-	-	-
Mode 18	149.85	Mode 16	152.36	1.68%	1.44%	2.47%	70.95%	0.83

Table 5: Substructuring results compared to the truth modes.

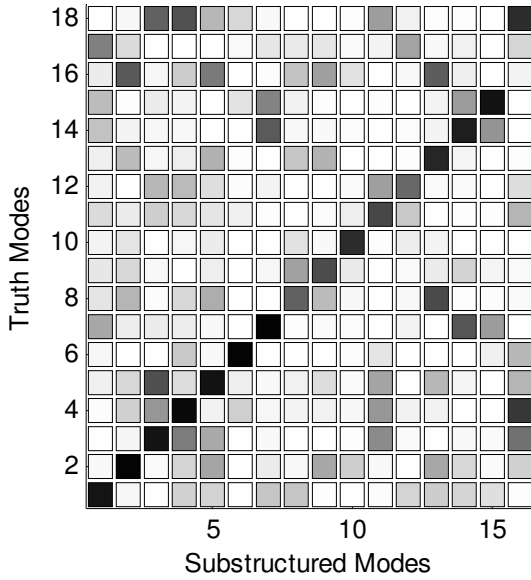


Figure 9: MAC between Truth and Substructured modes. Black = 1, White = 0.

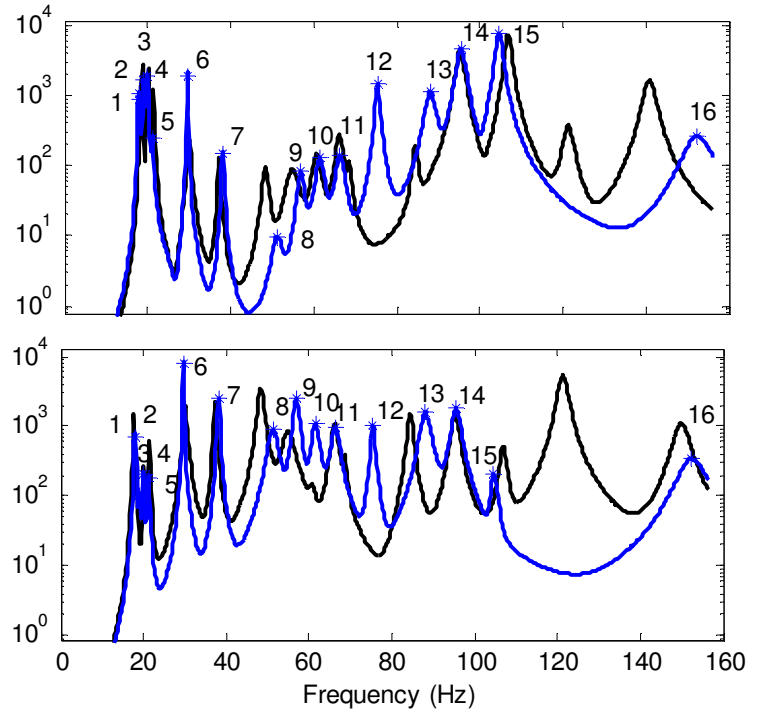
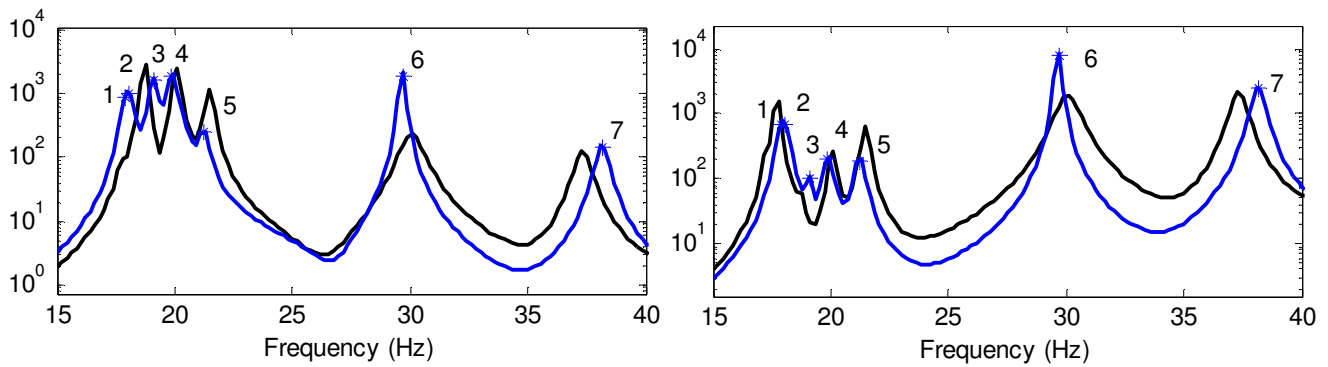


Figure 10: CMIFs from an  $x$ -direction pole reference (top) and a reference on the transmission simulator (bottom). The truth model shown in black and substructured model shown in blue.



**Figure 11: Zoom of Figure 10 showing the tight grouping of modes near 20 Hz. The CMIFs show an  $x$ -direction pole reference (left) and transmission simulator reference (right). Apart from damping errors, this frequency range is very well-behaved.**

Looking at Table 5, several trends are clear. The frequencies of the majority of the substructured modes are close to the truth model, within 5% error. Two notable examples are modes 8 and 12, each of which contributes significant error to the CMIFs in Figure 10. Mode 12 is significantly high and appears well separated from mode 11 in the substructured model, whereas it is very close to mode 11 in the truth model. Overall, the frequencies are accurate out to about 100 Hz. Above this range two high frequency truth modes at 121 Hz and 141 Hz were missed by the substructuring calculations. This can be seen clearly in the MAC of Figure 9 as the rows of the matrix that have low correlation to any of the columns. However, it is expected that the fidelity of the model would fall off in this range.

A comparison of the mode shapes shows good agreement as well. Over the majority of the frequency range, the MAC between the truth model and the substructured model is high. Even when the value of the MAC is low, the mode shapes bear a visual resemblance. Errors in the mode shapes yield scaling errors in the CMIFs of Figure 10, which are more pronounced in the region between 40 and 80 Hz, where the MACs tend to be low. These worst mode shapes are shown in Figure 13, compared to good mode shapes in Figure 12.

The substructured damping ratios are on the same order of magnitude as the measured damping ratios, but they are as much as 75% off. The effects of this can be seen in the CMIFs of Figure 11; mode 6 of the substructured model is significantly less damped than the corresponding measured model. There is a significant difference in the height of the two peaks even though the mode shapes are scaled similarly. Overall the damping ratios were worst aspect of the comparison, and were not predicted well at all. The turbine consists of many bolted joints and press fits. Notably, the blades are held in place primarily by the friction generated by the two sides of the black clamp. The hub is also pressed onto the mock generator shaft. These joints are likely not modeled well by the viscous damping assumed in these calculations, so it is reasonable that these values would be in error.

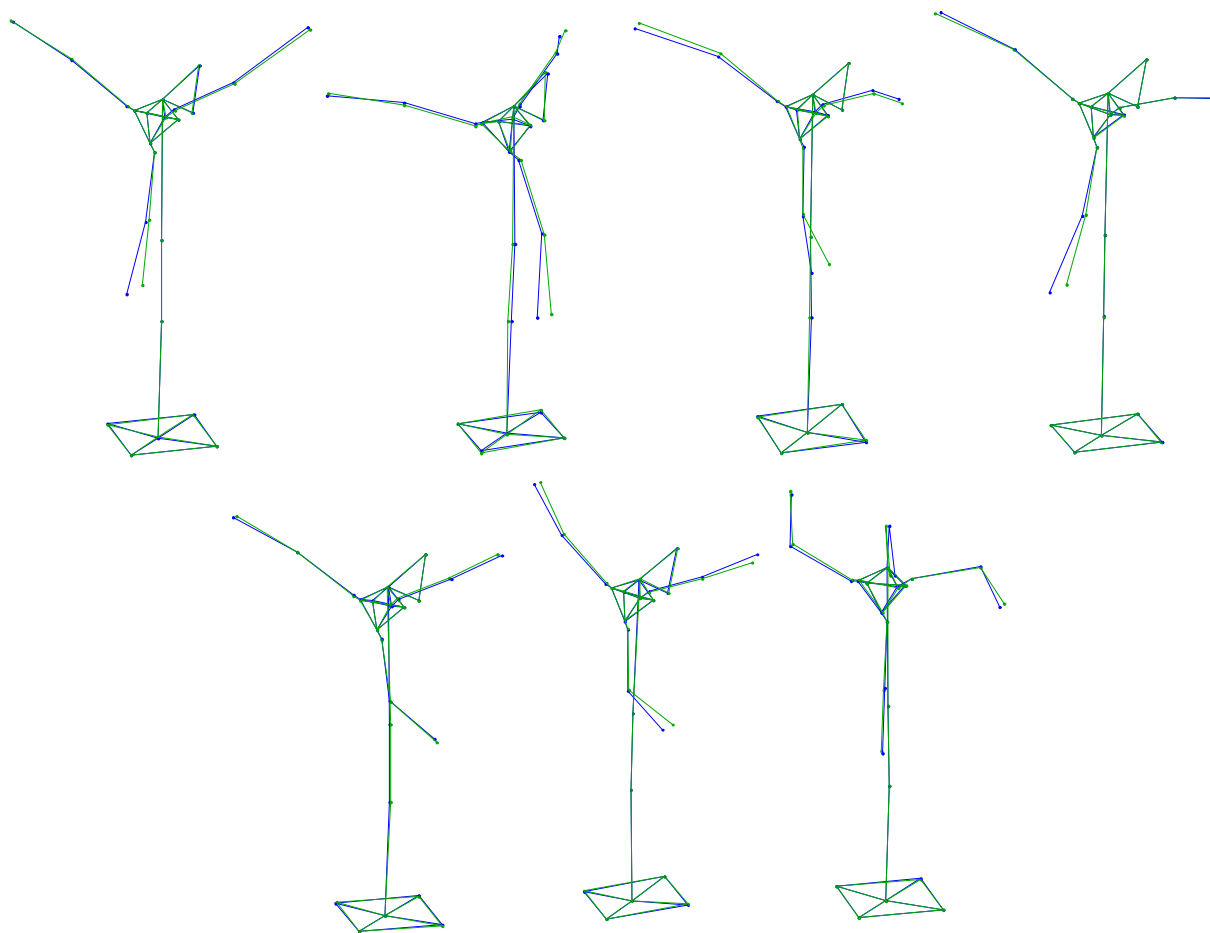


**Figure 12: Mode shapes with high MAC between substructured and truth data. From top left to bottom right, elastic modes 1 through 7.**

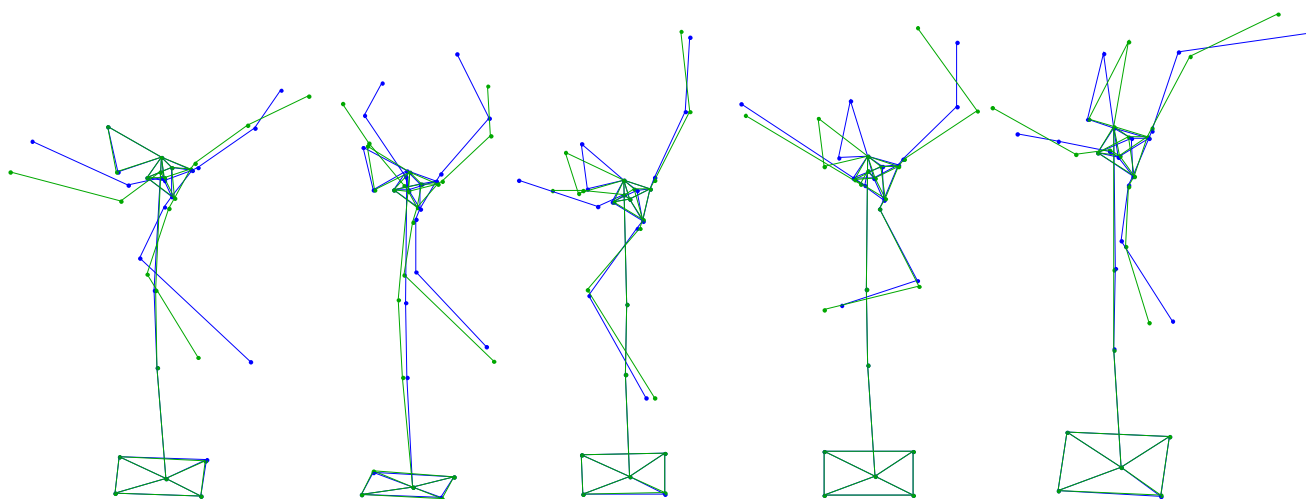


**Figure 13: From left to right, elastic modes 8 through 12. These shapes had the worst correlation to the truth data. Truth data is shown in blue, with substructured shapes overlaid in green.**

## 6. Possible Error Sources

Although the results for most modes are quite good, there is still up to 10% error in the frequencies of the system and MACs as low as 0.6. There is always the potential that these differences are due to nonlinearities of the system. It was seen that for both the blades and the tower substructures that the magnitude of displacement could shift the frequencies of the system (note the peaks in Figure 5 and Figure 8). For this reason, modal data taken from ‘soft’ drive points was viewed with suspicion, and often a different drive point would be selected to extract the mode as it was typically more linear. Nonlinearities could certainly cause the assembled system to behave slightly differently than a combination of the two substructures—for an equal force input, the deflections will be slightly different. Several other possible sources of error are considered here.

### 6.1. Accelerometer Mounting

Great care was taken in mounting the accelerometers so that they would be consistent throughout all the different measurements. Accelerometers were left in place between tests to ensure consistent mass-loading and orientation between tests. This should not be a significant source of error.

### 6.2. Mode Shape Scaling

Initially this effort utilized a very rough blade approximation as a triangular plate to estimate mass properties. It was seen that in this case, the first few elastic modes of the substructuring calculation were up to 15% off the truth data, which led to the creation of the more refined model appearing in this paper. To further investigate other modes that may be sensitive to the error, a brief sensitivity study was performed, which consisted of scaling the rotational inertia of the blades, and watching how the natural frequencies of each mode varied. The results are shown in Figure 14. Not surprisingly, the lower modes were more strongly affected by the moment of inertia. This agrees with an example in [7], where the low frequency modes contain large contributions from the rigid body mode shapes of the individual substructures. There are also three distinct peaks at modes 6, 9, and 12. These modes show a high sensitivity to scaling the blades’ inertia properties. It would seem that the majority of the sensitive natural frequencies were accurate in this study, which suggests that the mass properties used in the calculation are accurate.

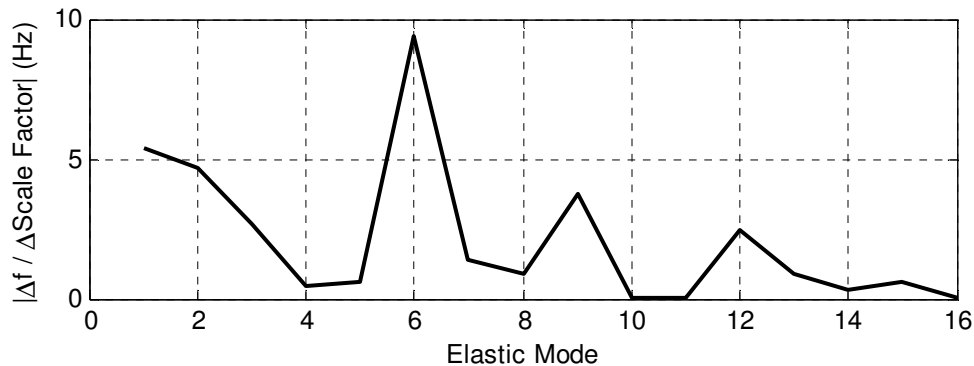


Figure 14: Sensitivity in the modes' natural frequencies to scaling the blades' rotational inertia.

### 6.3. Modal Truncation

The frequency of interest of the test was up to approximately 100 Hz, so the test proceeded up to 156 Hz to try to capture some of the modes above the frequency band to include in substructuring calculations. However, in this extra range only one mode was found in each subsystem that could be reasonably extracted. It is reasonable that the substructured model should not be accurate above that frequency range if each substructure only contains one mode, though this will largely be problem dependent.

### 6.4. Constraint Satisfaction

One additional source for potential error which is unique to the transmission simulator method is the satisfaction of the constraint equations. In the transmission simulator method, these constraints are softened, and satisfied in a least-squares fashion. In this specific example, the transmission simulator was assumed to be rigid in the frequency band of interest, since its first mode is near 1200 Hz. If the constraints are satisfied perfectly, the three transmission simulator models (one negative model and one from each substructure) will be moving in unison. Selected mode shapes of the substructured system are

shown in Figure 15. The discrepancies in motion are obviously small compared to the overall motion of each mode shape, so there should not be significant error from the constraints.

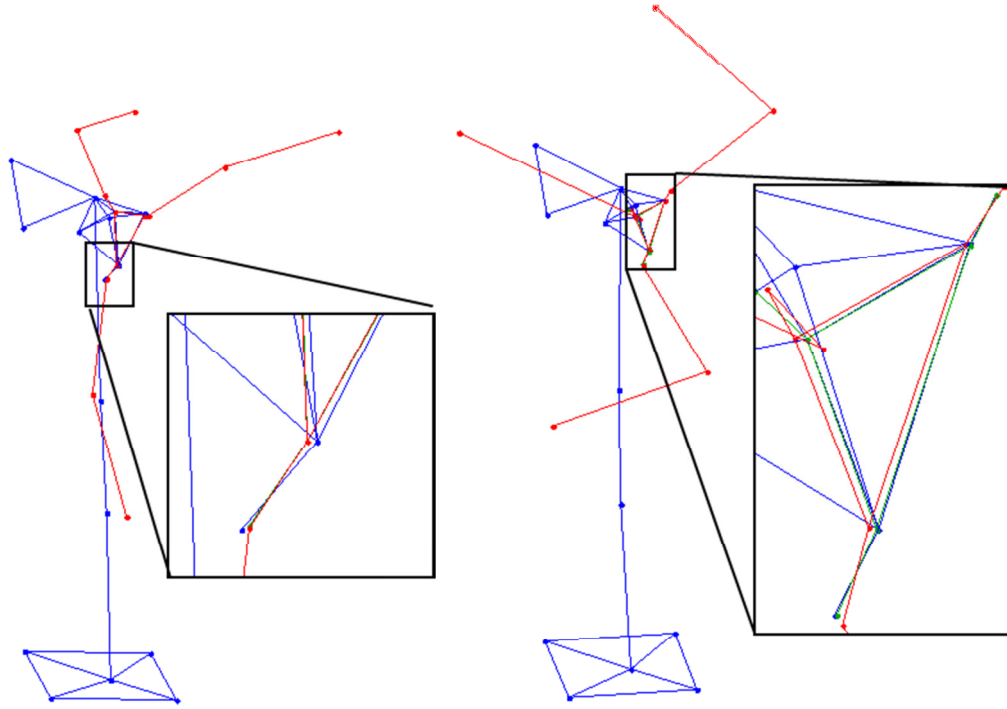


**Figure 15: Selected mode shapes showing small errors in the transmission simulator constraints. Degrees of freedom are colored according to their original substructure. Blue: Tower, Red: Blades, Green: Transmission Simulator. Elastic modes 6 and 11 are shown.**

## 7. Conclusions

This effort combined two experimental substructures consisting of components of the Ampair 600 Wind Turbine Test Bed. The blades were removed from the system to form the first substructure, and the second substructure consisted of the blades and the hub. A rigid transmission simulator consisting of only the hub was used to complete the substructuring. Rigid body modes of the tower system were measured experimentally, and the blade system rigid body modes were constructed analytically. The substructured model was compared to a truth model derived from a modal test of the entire turbine.

The rigid body modes and the first seven elastic modes were accurate by model correlation standards with frequency errors less than four percent and MACS above 0.92. Higher modes had frequency errors between 0.2 and 10 percent and MACS from 0.6 to 0.93. This range also demonstrated the most nonlinearity with obvious frequency shifts and damping changes from one impact reference to the next as shown in Figure 8. Damping errors in the predictions were worst, with fifty percent errors common. Future work that should be performed is characterization of the effect of the nonlinear joints on the estimate of viscous damping and mode shape errors. Modal truncation errors are apparent in the very high frequency band, but it is not known whether this is the cause of some of the errors in the mid-frequency band.

## REFERENCES

- [1] Mayes, Randall L., “An Introduction to the SEM Substructures Focus Group Test Bed – The Ampair 600 Wind Turbine”, *Proceedings of the 30<sup>th</sup> International Modal Analysis Conference*, Orlando, Florida, February 2012.
- [2] Harvey, Julie, and Aitavale, Peter, “Comparison of Some Wind Turbine Blade Tests in Various Configurations”, *Proceedings of the 30<sup>th</sup> International Modal Analysis Conference*, Orlando, Florida, February 2012.
- [3] Hensley, Daniel P., and Mayes, Randall L., “Extending SMAC to Multiple References”, *Proceedings of the 24<sup>th</sup> International Modal Analysis Conference*, pp.220-230, February 2006.
- [4] Rohe, Daniel P. and Allen, Matthew S., “Investigation into the Effect of Mode Shape Errors on Validation Experiments for Experimental-Analytical Substructuring”, *Proceedings of the ASME 2012 Int’l Design Engineering Technical Conferences & Computers and Information in Engineering Conference*, Chicago, Illinois, August 2012.
- [5] Mayes, Randall L. and Rohe, Daniel P., “Coupling Experimental and Analytical Substructures with a Continuous Connection Using the Transmission Simulator Method”, *Proceedings of the 31<sup>st</sup> International Modal Analysis Conference*, Garden Grove, California, February 2013.
- [6] Moshin, N. and Macknelly, D., “Modal Assessment of Wind Turbine Blade in Preparation of Experimental Substructuring”. *Proceedings of the 30<sup>th</sup> International Modal Analysis Conference*, Orlando, Florida, February, 2012.
- [7] Allen, Matthew S., Kammer, Daniel C., and Mayes, Randall L., “Uncertainty in Experimental/Analytical Substructuring Predictions: A Review with Illustrative Examples”, *Proceedings of the International Conference on Noise and Vibration Engineering*, Leuven, Belgium, 2010.